frontiers | Frontiers in Physics

TYPE Original Research
PUBLISHED 30 January 2025
DOI 10.3389/fphy.2025.1527070

OPEN ACCESS

EDITED BY
Woon-Seng Choong,
Berkeley Lab (DOE), United States

REVIEWED BY
Nancy Ford,
University of British Columbia, Canada
Goran Lovric,
Paul Scherrer Institut (PSI), Switzerland

*CORRESPONDENCE
Tiqiao Xiao,
tqxiao@sari.ac.cn

RECEIVED 12 November 2024
ACCEPTED 14 January 2025
PUBLISHED 30 January 2025

CITATION
Li K, Wang F, Xue Y, Huang S, Liu Z and Xiao T (2025) Move contrast X-ray imaging reveals wall infiltration along maize leaf vessels before water refilling.
Front. Phys. 13:1527070.
doi: 10.3389/fphy.2025.1527070

Move contrast X-ray imaging reveals wall infiltration along maize leaf vessels before water refilling

Ke Li[1], Feixiang Wang[1], Yanling Xue[1], Shiquan Huang[2], Zhixuan Liu[3] and Tiqiao Xiao[1]*

[1]Research Center for Shanghai Synchrotron Radiation Facility, Shanghai Advanced Research Institute, Chinese Academy of Sciences, Shanghai, China, [2]State Key Laboratory of Crop Stress Adaptation and Improvement, School of Life Sciences, College of Agriculture, Henan University, Kaifeng, China, [3]Hunan Rice Research Institute, Hunan Academy of Agricultural Sciences, Changsha, China

Research on the recovery mechanism of embolized vessels requires dynamic and sensitive observations of water refilling. The stable translation of the water/air interface was observed using X-ray absorption and phase contrast imaging. In this study, move contrast X-ray imaging (MCXI) was used to investigate the effect of the microstructure within microvessels on water refilling. Experimental verification using a maize leaf demonstrated that this method was approximately 12 times more sensitive than traditional transmission X-ray imaging. The pre-infiltration of water into the sieve pores of the side wall before water refilling was observed, which provided evidence of a deduction of two-step dynamic equilibrium during water refilling along cavitated vessels and water level rise in dynamic equilibrium instead of translating stably. Several quantitative analyses of the dynamic equilibrium were conducted owing to the high sensitivity of MCXI, making MCXI a promising tool to further investigate the micro-mechanism recovery of embolized vessels.

KEYWORDS

agent free imaging, x-ray imaging, water refilling, vessel cavitation, wall preinfiltration

1 Introduction

Water refilling plays a crucial role in plant physiology and eco-physiology [1, 2]. Water under tension is in a metastable state and prone to cavitation and embolism, which leads to the loss of hydraulic conductance, reduced productivity, and eventually plant death [1–3]. The mechanism by which embolized vessels are refilled with water and restored to their functional state has long eluded plant physiologists and physicists [4, 5]. Although several hypotheses have been put forward [3, 6, 7], the mechanisms of xylem embolism and refilling remain poorly understood due to technical limitations [8]. Dynamic and sensitive observations of water refilling along the xylem vessels are a practical way to achieve these goals.

Neutron imaging is a noninvasive imaging technique that is very sensitive to low-Z samples. Warren et al. used an isotope of water D_2O as a tracer to track the transport of water from the root to the stem [9]. Bouda et al. used magnetic resonance imaging (MRI) to successfully observe water transport in

a grapevine stem. The flow velocity along the vessels was measured without a contrast agent [10]. Nevertheless, these methods face challenges in both spatial and temporal resolution of the microvessels with diameters often less than 50 μm [11, 12].

Owing to its high penetration and high spatial resolution, transmission X-ray imaging (TXI) has been employed to investigate the microscopic evolution of embolism and repair in plants. The contrast of the TXI mainly originates from two aspects: the absorption of water in the vessels and the edge enhancement effect at the interface between water and air. Contrast agents are usually needed because the water in the vessels is too thin to generate efficient X-ray absorption. Kim and Lee reported significant work on bubble removal and embolism repair at a frame rate of 50 fps using a contrast agent and the phase contrast effect of the water/air interface [8, 13–15]. Contrast agents can interfere with the natural state of water refilling. The strength of the edge-enhancement effect depends on the thickness of the water. Additionally, the surrounding xylem tissues severely deteriorate the edge enhancement effect signals. Although the overlapping effect and structural evolution during water refilling can be removed by X-ray microtomography [16–18], the spatial and temporal resolutions still cannot compete with two dimensional imaging [19].

Recently, an agent-free X-ray imaging called move contrast X-ray imaging (MCXI) was developed, that can resolve weak signals in complex systems based on the movement of target media. The principles and characteristics of MCXI has been introduced in previous work [20–22]. Owing to the high sensitivity of MCXI, Xu and Li discovered a "temporal-spatial relay" refilling mode between adjacent vessels at initial stage of willow cuttage [23], and furthermore managed to measure the mass force field of the water in vessels [24]. Up to now, experiments have proved the advantages of MCXI in plant systems. Therefore, in this study, MCXI was applied to investigating the function of microstructure on the vessel side wall and the micro-mechanism of water refilling along the vessels in maize leaves. First, the feasibility and superiority of MCXI over traditional transmission X-ray imaging are demonstrated. The pre-infiltration of water into the sieve pores of the side wall before water refilling was observed, which provided evidence of a deduction of two-step dynamic equilibrium during water refilling along cavitated vessels and water level rise in dynamic equilibrium instead of translating stably. Several quantitative analyses of the dynamic equilibrium were conducted owing to the high sensitivity of MCXI. We believe that this method will be useful for applications of physics in biology, specifically plant physiology, and offers a new perspective on vascular recovery mechanisms, with potential implications for environmental physics, materials science, and biophysics.

2 Materials and methods

2.1 Sample preparation and data acquisition

The experiments were performed at the BL13HB X-ray Imaging and Biomedical Applications Beamline of Shanghai Synchrotron Radiation Facility (SSRF), a 3.5 GeV third generation light source. A schematic of the optical setup used in the experiment is shown in Figure 1A. A maize leaf was cut from the plant at the leaf joint with a sharp knife and then dried in air at an ambient temperature of 23°C with 40% humidity for 40 min. It was then fixed upright on a specially designed polymethyl methacrylate (PMMA) shelf, the bottom of which was a 5 × 5 × 1 cm water pool (Figure 1B). Using a remotely controlled syringe pump, 5 mL of water was injected into the pool once the X-ray array detector started recording the image sequence. A white LED lamp was also used to stimulate the transpiration of the leaf and improve the water refilling speed inside the xylem vessels. The X-ray photon energy was set to 15 keV and the detector was placed 15 cm away from the leaf to enlarge the edge-enhancement effect of X-ray imaging at the front end of the water refilling. The incident X-ray image on a scintillator (LuAG:Ce, 50 μm) was turned into visible light and then collected with an optical microscope (×10 magnification). Finally, the image sequence was recorded using a CMOS detector from HAMAMATSU (model: ORCA-Flash 4.0 C11440) with a physical pixel size of 6.5 μm and 2048 × 2048 pixel array. Considering the ×10 magnification of the optical system, the effective pixel size of the detector system was 0.65 μm. To focus on water refilling in a single xylem vessel, the high spatial resolution mode of the detector was selected for this experiment. The current measured by the ion chamber (Oxford, 140 mm long, filled with Nitrogen) was 5.3×10^{-6} A, and the beam size measured at the sample position is 2 mm (horizontal) × 1.6 mm (vertical). Accordingly, the photon flux density calculated is 8.75×10^{11} photons/mm^2/s, which implicates the entrance flux illuminated on the sample. All the absorbed photons contribute to the radiation dose and the dose of the sample equals to the entrance flux multiplied with absorption rate. In our case, the absorption of maize leaf is very weak at the monochromatic hard X-ray photon energy used in the experiments. This means that the radiation dose imposed on the sample is very limited. Compromising the water refilling speed, detector frame rate, and SNR of each image frame, the exposure time was set to 0.5 s, which infers to a frame rate of 2 fps. From the beginning of the water injection into the pool, we recorded 64 s and 128 frames of water refilling in the maize leaf. The entire sequence is shown in Supplementary Video 1 as a video file in Supplementary Material.

2.2 Principle of move contrast X-ray imaging

For the convenience of theoretical analysis for move contrast X-ray imaging (MCXI), a Cartesian coordinate system was established at the projection image plane, such that every point in the image had its own spatial coordinates (x, y), and the grayscale image can be described as $g(x, y)$. If the projection images are collected by the X-ray detector at a frame rate of f_{ac} (frames/s), the grayscale value at time t can be expressed as $g(x, y, t)$, which fluctuates over time. The fluctuation of the grayscale value in the projected images usually results from the movement of the medium of interest inside the samples, the movement of components surrounding the medium of interest, and random noise. Although the effects of these factors are entangled in real space, it is possible to separate them using a time-domain frequency analysis. Accordingly, for the grayscale value at point (x, y) in the projected images, a Discrete Fourier Transform

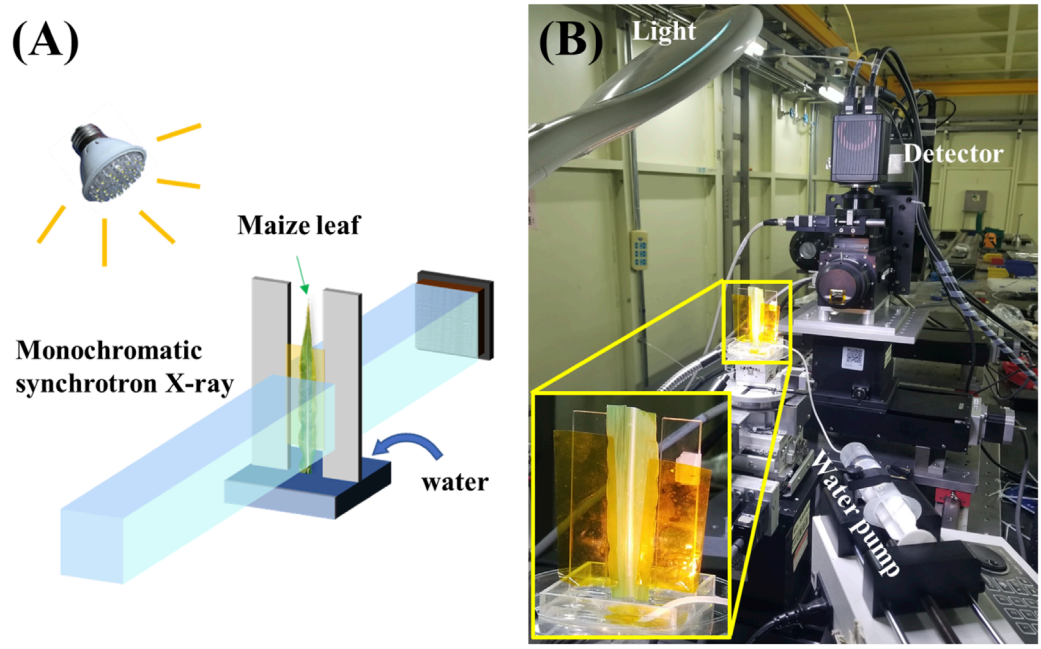

FIGURE 1
Data acquisition for move contrast X-ray imaging indicating water refilling in a maize leaf. **(A)** Diagram indicating the experimental setup. **(B)** Photograph of the experimental apparatus at BL13HB of SSRF.

was conducted for $g(x, y, t)$, and we obtain

$$\mathcal{G}(x,y,k) = \sum_{t=0}^{t_{N-1}} g(x,y,t)\cos\left(\frac{2\pi kt}{t_N}\right) - j\sum_{t=0}^{t_{N-1}} g(x,y,t)\sin\left(\frac{2\pi kt}{t_N}\right) \quad (1)$$

where $G(x, y, k)$ represents the Discrete Fourier Transform of $g(x, y, t)$, t_N is the total length of time for the image sequence, and $t_N = T \times N$, where T is the time period of image acquisition, and N is the total frame number. k is an integer ranging from 0 to N. However, considering that the cosine is even symmetric, while the sine has odd symmetry, $G(k)$ and $G(N\text{-}k)$ are conjugates of each other. Therefore, k is usually limited to the range of 0 to $N/2$, and represents the time-domain frequency with $f_k = k/T$.

According to Equation 1, the amplitude and phase spectrum can be obtained with Equations 2, 3.

$$A(x,y,k) = \sqrt{\mathrm{Re}^2(\mathcal{G}(x,y,k)) + \mathrm{Im}^2(\mathcal{G}(x,y,k))} \quad (2)$$

$$\varphi(x,y,k) = \arctan\frac{\mathrm{Im}(\mathcal{G}(x,y,k))}{\mathrm{Re}(\mathcal{G}(x,y,k))} \quad (3)$$

In this manner, the amplitude and phase distribution of $G(x, y, k)$ in the real space (x, y) and time-domain frequency space (k) can be obtained in the Amplitude image (following Section 2.2.1) and Phase image (supplementary methods in Supplementary Material), as long as the process of media movement is sampled into a sequence of projection images over a period of time at an appropriate frame rate. $G(x, y, k)$ results from the grayscale variation introduced by the media movement inside the sample and is defined as the move contrast. The distribution of $G(x, y)$ in real space integrated with a frequency-band filter forms a moving contrast image.

2.2.1 Amplitude image of MCXI

Media movement in the region of interest results in grayscale variations in the recorded image sequence. Different moving modes lead to different frequency distributions of $G(x, y, k)$ in the time-domain frequency space. The amplitude was expanded by the spectrum as follows:

$$\begin{aligned} A(x,y) &= A(x,y,0) + \sum_{k=1}^{k_L-1} A(x,y,k) + \sum_{k=k_L}^{k_U} A(x,y,k) + \sum_{k=k_U+1}^{N/2} A(x,y,k) \\ &= A_{ZFC}(x,y) + A_{LFC}(x,y) + A_{IFC}(x,y) + A_{HFC}(x,y) \end{aligned} \quad (4)$$

where $A_{ZFC}(x, y)$ refers to the zero-frequency component for the static background of the image sequence, $A_{LFC}(x, y)$ stands for low-frequency components due to the movement of media in the low-frequency band, $A_{HFC}(x, y)$ denotes high-frequency components due to the movement of media at high frequency or random noises, $A_{IFC}(x, y)$ is the component at a specified frequency band (k_L, k_U) for the media of interest. Similarly, move contrast imaging (MCI) in media of interest follows the same reconstruction process by extracting signals in a given frequency band. According to Equation 4, each component can be imaged separately, and the interference between components is eliminated. Therefore, the sensitivity of MCI can be improved significantly.

2.2.2 Scan mode of MCXI

A typical move contrast image is reconstructed with all image sequence which reveals the entire track of the target media. Whereas if a window is used to select a portion of the entire sequence for move contrast analysis, only the motion information during this time period will be extracted. While this window is moving in the

chronological direction throughout the entire sequence, multiple move contrast images are generated and naturally form a video, which contains the moving information of the front end. Therefore, we call it the scan mode of MCXI. When a window of length L is scanned forward in steps of S frames at a time on a sequence with a total number of frames of N, the total number of frames of the video generated by the scan mode is (N-L)/S. The size of L affects the signal-to-noise ratio of the results, in that smaller L tends to contain the information of the front end only, but also results a lower signal-to-noise ratio. The step size S affects the temporal resolution of the dynamic pattern, when S = 1, the temporal resolution is the same as the original projection, but at the same time, it means higher computational cost.

3 Results

One of the frames in the image sequence is shown in Figure 2A. Three vessels are observed in the middle of the image. Two thicker vessels on both sides are metaxylem vessels (approximately 30 μm in diameter), while the thinner one in the middle is a protoxylem vessel (approximately 12 μm in diameter). The position and structure of these vessels can be confirmed using high-resolution CT, as shown in Supplementary Figure S1 of the Supplementary Material. It is difficult to distinguish whether a vessel has been filled with water or not and where the water level is, even if the display range of the image has been stretched to a maximum to increase contrast and visibility. The absorption of 15 keV X-ray by 30 μm water is only 0.5%, which cannot produce sufficient absorption contrast. However, the edge enhancement effect at the water level is buried in the xylem background; thus, it is difficult to observe where the water arrives. MCXI was introduced to solve the dilemma of absorption and phase contrast of traditional TXI. As shown in Figure 2B, the amplitude image of MCXI was acquired using a sequence of 128 images with a time-frequency window of 0.0156 Hz–0.0938 Hz (corresponding k from 1 to 6). By comparing Figure 2B with A, the water refilling route is revealed, and it is evident that the signal-to-noise ratio of MCXI is improved significantly. However, the weak signal of small water drops infiltrating the surrounding tissues into an empty vessel was well preserved and enhanced, as indicated by the yellow arrow in Figure 2B. To quantitatively evaluate the sensitivity of the two methods, the contrast-to-noise ratio (CNR) [25] was calculated using a white rectangular section. The CNR value of MCXI was 6.52, while that of TXI was 0.54. In this case, the image quality improvement using MCXI increased 12-fold compared to TXI, demonstrating a much higher sensitivity to weak signals and robustness against noise. Detailed calculation of the CNR value is given in Supplementary Figure S1 of Supplementary Material.

As depicted in Figure 2B, gaps were regularly distributed along the track imaged by the MCXI. According to the high-resolution CT image shown in Supplementary Figure S2 of Supplementary Material, there is a series of annular microstructure inside the vessels of a maize leaf that acts as nodes to decelerate water refilling and opens breaches for water exchange between the vessel and adjacent tissues. To further compare the images obtained using TXI and MCXI, grayscale profiles along the lines indicated in Figures 2A, B are shown in Figure 2C, which indicates the sections of the imaged tracks and the related background. As shown in Figure 2C, the remarkable peak in the red line indicates a distinct track of water refilling, which is barely visible in the blue line. Moreover, the diameter of the water refilling track in the MCXI was 30.6 μm, which is the same as the result measured using TXI. Therefore, MCXI has high spatial precision and greatly improved sensitivity.

Considering the high sensitivity of MCXI, we further explored water refilling along the xylem vessels. To increase the temporal resolution, the scan mode of MCXI used a short sequence of 16 frames and a step of 1 frame, rather than the entire image sequence. A local region of interest was selected, and the reconstructed results using the four time periods are shown in Figures 3A–D. From Figures 3A, B, the water level stagnated at the position of a node within the xylem vessel, where only a thin layer of water appeared on the left wall. According to measurements, the thickness of the water layer was 6 μm, but the height reached an astonishing 38 μm, even longer than the diameter of the xylem. However, this characteristic structure was not observed in TXI at t = 14.0 s (Figure 3E). The reason why this thin water film has not been observed before might be a combination of two aspects. This layer of water may be too thin to generate an efficient edge-enhancement effect, or this phenomenon may be due to the irregular surface of the water layer. The intensity profiles along the lines indicated in Figures 3B, E are shown in Figure 3F. The center of this water layer is located on the left side wall of the xylem vessel, which indicates that before water refills a dry vessel, very little water infiltrates the side wall in advance to a significant altitude.

Finally, according to the temporal evolution from Figures 3A–D, the water level rises in dynamic equilibrium instead of stable translation. The procedure of water refilling cavitated vessels can be inducted as a two-step circulation: First, from Figures 3A–C, the water level halted at a node in the vessel until a small amount of water infiltrated the sieve pores on the side wall and reached the next node (cribrate microstructure of 3D CT result in Supplementary Figure S1 of Supplementary Material) due to capillarity. Second, from Figures 3C, D, the excessive superficial area of the water front end caused strong surface tension, which pulled water up to form a relatively balanced concave profile. By repeating these two steps, the water refills the cavitated vessels, similar to climbing a ladder with two hands. By scanning a total of 128 frames with MCXI scan mode, we can generate a movie depicting water transport along the vessel, as shown in Supplementary Video 2 as a video file in Supplementary Material.

To prove the deduction of a two-step dynamic equilibrium during water refilling mentioned above, we recorded the height coordinates of the front ends of water refilling and wall infiltration in every frame of Supplementary Video 2, and plotted the entire process of cavitated vessel recovery in Figure 4A. The horizontal axis represents time, whereas the vertical axis represents the vertical position of water refilling (blue curve) and wall penetration (red curve). The red curve was always above the blue curve, indicating that wall infiltration before water refilling is a common phenomenon in xylem vessels. The red curve presents a clear stepwise upward trend, indicating that the wall infiltration exhibits periodic stalls. Comparing the trajectory of water refilling in Figure 2B with this curve, the stalls of wall infiltration mostly occurred at positions where the annular nodes were located inside the xylem vessel (indicated by the gray dashed lines). Similarly, the blue curve

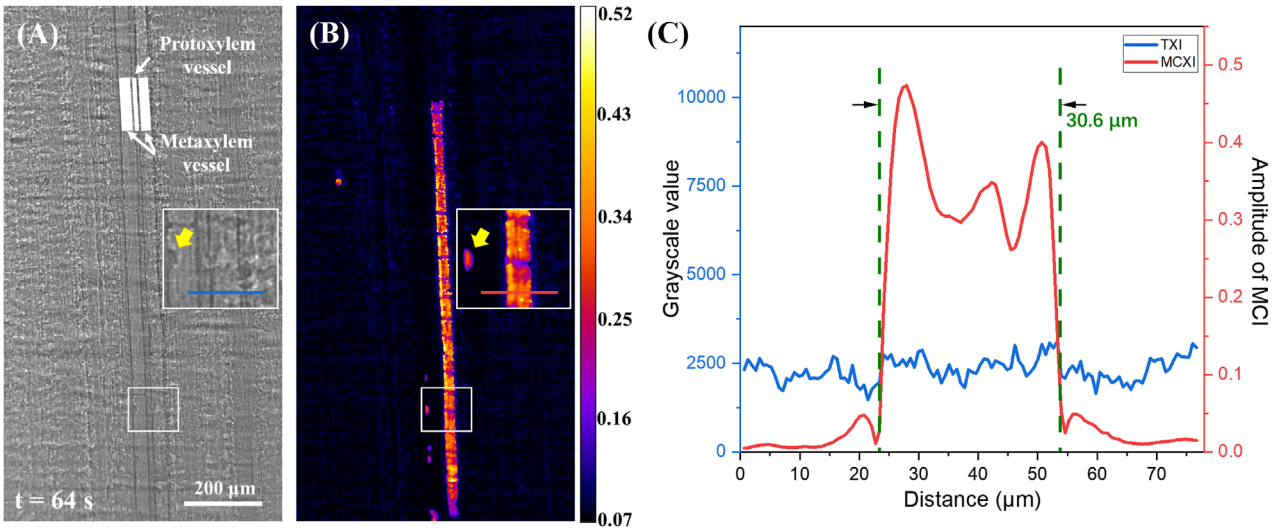

FIGURE 2
Comparison between transmission X-ray imaging and move contrast X-ray imaging used to observe water refilling along a xylem vessel in a maize leaf. **(A)** Transmission X-ray image captured at 64.0 s, scale bar 200 μm. **(B)** Amplitude image using MCXI from 0 s to 64 s. **(C)** Intensity profiles at two lines noted in **(A, B)**, respectively.

shows fluctuations at the same height; however, its amplitude is smaller than that of the red curve. This suggests that the surface of the water also encounters obstacles when passing through the annular nodes. Since the wall of the vessel was pre-infiltrated by water, the water refilling process was smoother. By calculating the height difference between the red and blue curves in Figure 4A, we obtained the distance between wall infiltration and water refilling with respect to time (Figure 4B). It can be observed from the figure that the advantage varies periodically with time, increasing and then decreasing. The maximum value of each cycle was close to the length of the corresponding segment, indicating that wall infiltration led to water refilling in one segment of the vessel when the curve reached a local maximum value. In contrast, when the curve reached a local minimum value, water was quickly pulled closer to the front end of the wall infiltration under strong surface tension. This periodic change between the maximum and minimum values corresponds to the two-step dynamic equilibrium of the water transport, as summarized in Figure 3. In addition, there are 19 obvious maximum values in Figure 4B, which is consistent with the fact that the entire vessel in Figure 2 is divided into 19 segments by 18 annular nodes. Therefore, the time period of this two-step dynamic equilibrium within the time range of 8–64 s can be calculated to be approximately 3 s.

Based on the MCXI phase analysis in Supplementary Figure S3 (Supplementary Material), the average speed of the water rise during the entire process is approximately 17 μm/s. However, the instantaneous speeds in local areas are more valuable for studying the mechanism of recovery of embolized vessels. Therefore, by differentiating the position-time curves in Figure 4A, we observed the relationships between instantaneous speed, time of water refilling, and wall infiltration (Figure 5A). Although the mean values of instantaneous speeds of water refilling and wall infiltration are similar (18.03 μm/s versus 17.57 μm/s), the standard deviation of the latter is about two times larger than the former (7.89 versus 14.80 μm/s). Visually, wall infiltration frequently switches between high-speed motion and stagnation, whereas water refilling also exhibits periodic fluctuations; however, the amplitudes are smaller. In addition, by comparing the moments when the red and blue curves in Figure 5A reach the local maximum and minimum values, we can see that water refilling lags wall infiltration by 1–1.5 s. Considering that the time period of the two-step dynamic equilibrium is approximately 3 s, there are several instances in Figure 5A where the valleys of the red curve correspond to the peaks of the blue curve, such as at 12.5, 16.5, 45.5, and 60.0 s. To explore the effect of the annular nodes inside the vessel on the instantaneous speed, we combined the spatial position information in Figure 4A with the speed information in Figure 5A to obtain the spatial distribution of the instantaneous speeds of water refilling and wall infiltration, as shown in Figure 5B. At the positions of the annular nodes, the speed of wall infiltration generally drops to zero, while the speed of water refilling mostly decreases to 10 μm/s, and in some cases, it does not even decrease at the positions of the annular nodes. This suggests that the annular nodes may hinder both water refilling and wall infiltration; however, the effect on wall infiltration is more pronounced. Once water passes through the annular nodes, the speed of wall infiltration increases more noticeably than that of water refilling, and reaches the maximum instantaneous speed at the midpoint between the two annular nodes. After statistically analyzing the maximum instantaneous speeds within the 19 segments of the pipe divided by the annular nodes, over 83% of the maximum instantaneous speeds of wall infiltration reach 30 μm/s, with a few reaching 60 μm/s. In comparison, the average maximum instantaneous speed per segment of the vessel for water refilling is only 26.5 μm/s.

The inconsistency in the rising speed of water at different heights in the vessels prompted us to further investigate possible reasons for this phenomenon. We analyzed the local maximum values of the water refilling and wall infiltration speeds (Figure 5B) and the

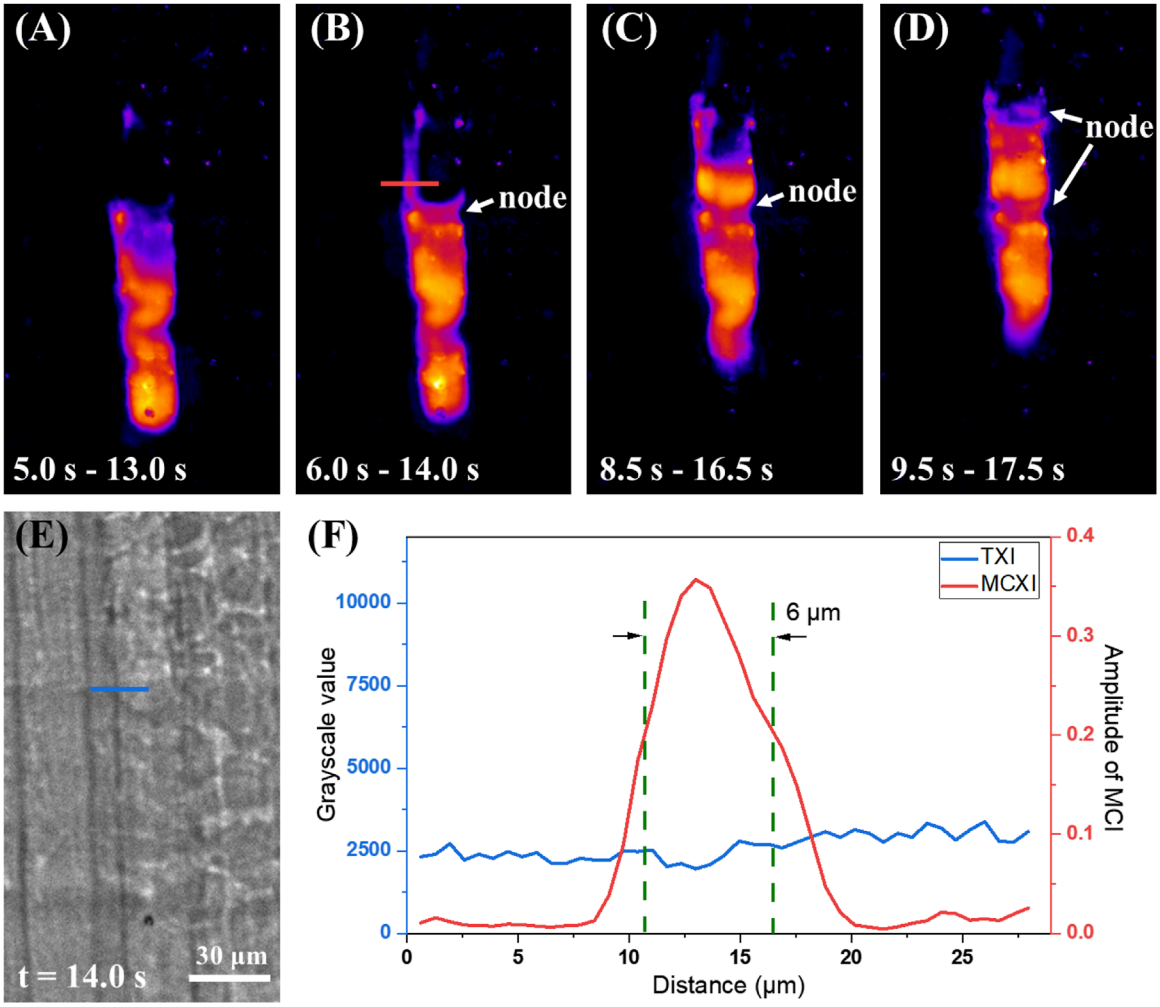

FIGURE 3
Direct observation of wall infiltration before water refilling with MCXI. **(A–D)** MCXI results at 5.0–13.0 s, 6.0–14.0 s, 8.5–16.5 s, and 9.5–17.5 s **(E)** TXI projection at 14.0 s, scale bar 30 μm. **(F)** Intensity profiles at two lines noted in **(B, E)**, respectively.

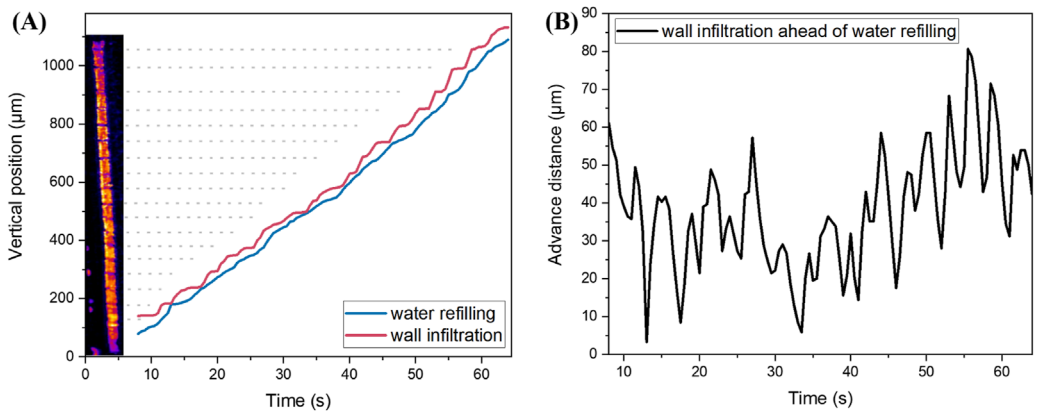

FIGURE 4
Quantitative description of wall infiltration before water refilling. **(A)** Vertical position of water refilling and wall infiltration versus time. **(B)** Advance distance between wall infiltration and water refilling versus time.

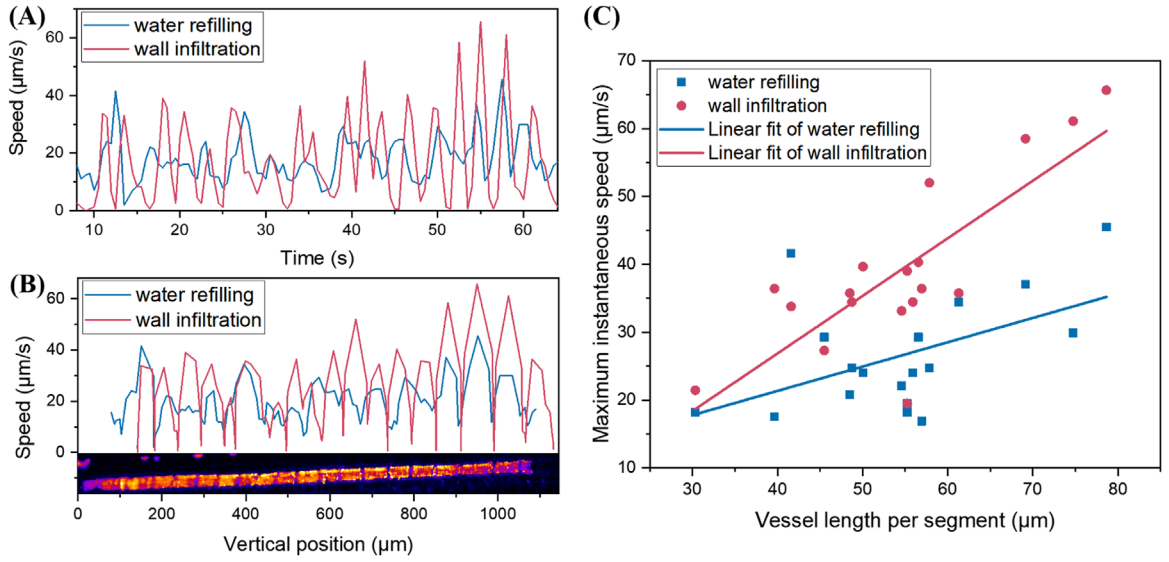

FIGURE 5
Instantaneous speed analyses of water refilling and wall infiltration. **(A)** Instantaneous speed versus time. **(B)** Instantaneous speed versus vertical position. **(C)** Local maximum speed of water refilling and wall infiltration in **(B)** and their corresponding segment lengths of the vessel.

corresponding segment lengths of the vessel (Figure 5C). Visually, the longer the segment length divided by the annular nodes, the greater the maximum instantaneous speed of water refilling and wall infiltration. This suggests that the water accelerates before being impeded by the annular nodes; thus, the length of each vessel segment has a positive impact on the maximum instantaneous speed. After performing a linear fit to the two sets of scatter plots, wall infiltration exhibited a larger slope than water refilling, indicating that wall infiltration has a higher accelerating rate when transmitting the same distance and is more likely to reach a higher instantaneous speed. Of course, considering that the R^2 value for the red scatter plot after the linear fit was 0.64, while only 0.25 for the blue scatter plot, the accuracy of the linear fit for wall infiltration was higher. It should be noted that this linear pattern is not applicable when the length of each vessel segment becomes very large, because there must be an upper limit to the speed of water refilling and wall infiltration, even without the impediment of annular nodes.

The structural integrity of the annular nodes within the conduits impacts water transport through vessels. For example, the annular nodes between the vertical position of 380 μm and 460 μm in the vessel (Figure 5B) do not have a clear structure, which may be a natural defect during plant growth. This may explain why the instantaneous speed within the corresponding segment of the vessel (Figure 5B) did not follow a periodic rule. Additionally, the points in Figure 5C that significantly deviate from the linear fit results may also have been caused by structural defects in the annular nodes within the conduits.

4 Discussion

Research on the mechanism by which embolized vessels recover requires dynamic and sensitive observation of water refilling *in vivo*. Conventional transmission X-ray imaging using absorption contrast or phase contrast faces difficulties with low contrast and weak signals when water refilling occurs in thin vessels. In this study, move contrast X-ray imaging was used to investigate the characteristics of water refilling along microvessels. While traditional phase imaging taking the advantage of high sensitivity response to the density difference between different components of the sample, MCXI uses the grayscale variation of the image to track the moving target. As the time-domain frequency signal is used, MCXI has the ability to track subtle signals in a complicated background. The feasibility and validity of MCXI were demonstrated by comparison with traditional TXI in maize leaves. MCXI has been proven to be 12 times more sensitive to weak signals compared to TXI. Finally, pre-infiltration of water into the sieve pores of the side wall before water refilling was observed, which provides evidence of a two-step dynamic equilibrium deduction during water refilling along cavitated vessels and water level rise in dynamic equilibrium instead of stable translation.

Several analyses of the two-step dynamic equilibrium were conducted. The time period for this two-step dynamic equilibrium was approximately 3 s. Although the mean instantaneous speeds of water refilling and wall infiltration were similar, the standard deviation of the wall infiltration speed was significantly higher, with more frequent changes in speed. There was a lag of 1–1.5 s between the peaks of water refilling and wall infiltration, with wall infiltration generally reaching higher speeds. While both processes are hindered by annular nodes within the vessels, wall infiltration is more affected; however, once water passes through the nodes, the speed of wall infiltration increases more noticeably compared to water refilling. Finally, further investigation into the inconsistency in the rising speeds of water at different heights in the vessels revealed that the length of each vessel segment had a positive impact on the maximum instantaneous speeds, with wall infiltration exhibiting a

higher acceleration rate and reaching higher instantaneous speeds, with a higher accuracy in the linear fit compared to water refilling.

There are also some limitations to the MCXI that should be noted. The source of the moving contrast is the variation in intensity recorded by the detectors, which is generated by the modulation of the moving media to the transmitting light field. Therefore, if the vessel is already filled with water, the subsequent water transport is invisible during MCXI. Since water is homogeneous, no intensity fluctuations can be captured by the detectors. In addition, MCXI requires a sequence of images to perform a Fourier transform in the time domain. Owing to the nature of the Fourier transform, temporal precision is associated with the number of images in the sequence. Therefore, MCXI requires detectors with higher frame rates to obtain a finer frequency analysis. According to the same principle, the precision of the instantaneous speed calculated by the scan mode of the MCXI also relies on the frame rate. Therefore, using a brighter X-ray light source improves the temporal resolution of MCXI.

Taken together, this study reports that the annular structure within the plant vessel plays an important role in the recovery process after cavitation, in addition to enabling the plant to maintain its shape during drought and water deficit. The annular nodes help to continuously refill the entire vessel with water through a two-step dynamic equilibrium process when the transpiration pull does not function. Considering the high sensitivity and signal-to-noise ratio of MCXI, the proposed method will be useful for applications of physics in biology, specifically plant physiology, and offers a new perspective on vascular recovery mechanisms, with potential implications for environmental physics, materials science, and biophysics.

Data availability statement

The raw data supporting the conclusions of this article will be made available by the authors, without undue reservation.

Author contributions

KL: Data curation, Methodology, Validation, Writing–original draft, Writing–review and editing. FW: Data curation, Investigation, Methodology, Validation, Writing–original draft. YX: Formal Analysis, Investigation, Software, Writing–review and editing. SH: Formal Analysis, Resources, Validation, Writing–review and editing. ZL: Investigation, Validation, Writing–review and editing. TX: Funding acquisition, Methodology, Project administration, Writing–review and editing, Writing–original draft.

Funding

The author(s) declare that financial support was received for the research, authorship, and/or publication of this article. This study was funded by the CAS Project for Young Scientists in Basic Research (YSBR-096), The National Key Research and Development Program of China (Grant Nos. 2022YFA1603601, 2021YFF0601203, and 2021YFA1600703) and the Young Scientists Fund of the National Natural Science Foundation of China (Grant No. 12405376 and 12205361).

Acknowledgments

The authors thank Honglan Xie, Biao Deng, Xiaolu Ju, Guohao Du and Han Guo for their kind help and fruitful discussions on the experiments and data processing.

Conflict of interest

The authors declare that the research was conducted in the absence of any commercial or financial relationships that could be construed as a potential conflict of interest.

Generative AI statement

The author(s) declare that no Generative AI was used in the creation of this manuscript.

Publisher's note

Supplementary material

The Supplementary Material for this article can be found online at: https://www.frontiersin.org/articles/10.3389/fphy.2025.1527070/full#supplementary-material

References

1. Brodribb TJ. Xylem hydraulic physiology: the functional backbone of terrestrial plant productivity. *Plant Sci* (2009) 177(4):245–51. doi:10.1016/j.plantsci.2009.06.001

2. Tyree MT, Salleo S, Nardini A, Gullo MAL, Mosca R. Refilling of embolized vessels in Young stems of laurel. Do we need a new paradigm? *Plant Physiol* (1999) 120(1):11–22. doi:10.1104/pp.120.1.11

3. Nardini A, Gullo MAL, Salleo S. Refilling embolized xylem conduits: is it a matter of phloem unloading? *Plant Sci* (2011) 180(4):604–11. doi:10.1016/j.plantsci.2010.12.011

4. Holbrook NM, Ahrens ET, Burns MJ, Zwieniecki MA. *In vivo* observation of cavitation and embolism repair using magnetic resonance imaging. *Plant Physiol* (2001) 126(1):27–31. doi:10.1104/pp.126.1.27

5. Sabella E, Aprile A, Genga A, Siciliano T, Nutricati E, Nicolì F, et al. Xylem cavitation susceptibility and refilling mechanisms in olive trees infected by xylella fastidiosa. *Scientific Rep* (2019) 9(1):9602. doi:10.1038/s41598-019-46092-0

6. Salleo S, Lo Gullo M, Trifilo P, Nardini A. New evidence for a role of vessel-associated cells and phloem in the rapid xylem refilling of cavitated stems of laurus nobilis L. *Plant Cell and Environ* (2004) 27(8):1065–76. doi:10.1111/j.1365-3040.2004.01211.x

7. Trifilò P, Kiorapostolou N, Petruzzellis F, Vitti S, Petit G, Gullo MAL, et al. Hydraulic recovery from xylem embolism in excised branches of twelve woody species: relationships with parenchyma cells and non-structural carbohydrates. *Plant Physiol Biochem* (2019) 139:513–20. doi:10.1016/j.plaphy.2019.04.013

8. Ryu J, Hwang BG, Lee SJ. *In vivo* dynamic analysis of water refilling in embolized xylem vessels of intact zea mays leaves. *Ann Bot* (2016) 118(5):1033–42. doi:10.1093/aob/mcw145

9. Warren JM, Bilheux H, Kang M, Voisin S, Cheng C-L, Horita J, et al. Neutron imaging reveals internal plant water dynamics. *Plant and Soil* (2013) 366(1-2):683–93. doi:10.1007/s11104-012-1579-7

10. Bouda M, Windt CW, McElrone AJ, Brodersen CR. *In vivo* pressure gradient heterogeneity increases flow contribution of small diameter vessels in grapevine. *Nat Commun* (2019) 10(1):5645–10. doi:10.1038/s41467-019-13673-6

11. Rolland V, Bergstrom DM, Lenné T, Bryant G, Chen H, Wolfe J, et al. Easy come, easy go: capillary forces enable rapid refilling of embolized primary xylem vessels. *Plant Physiol* (2015) 168(4):1636–47. doi:10.1104/pp.15.00333

12. Takanashi T, Kawamura H, editors Evaluation of spatial resolution of mri, optical ct and X-ray ct using mtf for gel dosimeter. In *World congress on medical physics and biomedical engineering 2018*. Springer (2019).

13. Lee S-J, Kim Y. *In vivo* visualization of the water-refilling process in xylem vessels using X-ray micro-imaging. *Ann Bot* (2008) 101(4):595–602. doi:10.1093/aob/mcm312

14. Kim HK, Lee SJ. Synchrotron X-ray imaging for nondestructive monitoring of sap flow dynamics through xylem vessel elements in rice leaves. *New Phytol* (2010) 188(4):1085–98. doi:10.1111/j.1469-8137.2010.03424.x

15. Xue Y, Xiao T, Du G, Tong Y, Liu H, Deng B, et al. Observation of cavitation and water-refilling processes in plants with X-ray phase contrast microscopy. *Nucl Sci Tech* (2013) 24(6). doi:10.13538/j.1001-8042/nst.2013.06.001

16. Brodersen CR, McElrone AJ, Choat B, Matthews MA, Shackel KA. The dynamics of embolism repair in xylem: *in vivo* visualizations using high-resolution computed tomography. *Plant Physiol* (2010) 154(3):1088–95. doi:10.1104/pp.110.162396

17. Xu L, Chen R, Du G, Yang Y, Wang F, Deng B, et al. Anisotropic shrinkage of insect air sacs revealed *in vivo* by X-ray microtomography. *Sci Rep* (2016) 6:32380. doi:10.1038/srep32380

18. Knipfer T, Cuneo IF, Brodersen CR, McElrone AJ. *In situ* visualization of the dynamics in xylem embolism formation and removal in the absence of root pressure: a study on excised grapevine stems. *Plant Physiol* (2016) 171(2):1024–36. doi:10.1104/pp.16.00136

19. Suuronen J-P, Peura M, Fagerstedt K, Serimaa R. Visualizing water-filled versus embolized status of xylem conduits by desktop X-ray microtomography. *Plant Methods* (2013) 9(1):11. doi:10.1186/1746-4811-9-11

20. Wang F, Zhou P, Li K, Mamtilahun M, Tang Y, Du G, et al. Sensitive imaging of intact microvessels *in vivo* with Synchrotron radiation. *IUCrJ* (2020) 7(5):793–802. doi:10.1107/s2052252520008234

21. Wang F, Li K, Xu M, Ju X, Xiao T. Move contrast X-ray imaging and its applications. *Nucl Instrum Methods Phys Res Sect A* (2023) 1055:168560. doi:10.1016/j.nima.2023.168560

22. Ju X, Li K, Yu F, Xu M, Deng B, Li B, et al. Move contrast X-ray imaging of electrochemical reaction process in electrolytic cell. *Acta Phys Sin* (2022) 71:144101. doi:10.7498/aps.71.20220339

23. Xu M, Li K, Xue Y, Wang F, Liu Z, Song Z, et al. Water refilling along vessels at initial stage of willow cuttage revealed by move contrast ct. *Front Phys* (2023) 11:11. doi:10.3389/fphy.2023.1174387

24. Xu M, Li K, Xue Y, Wang F, Liu Z, Xiao T. Measurement of mass force field driving water refilling of cuttage. *Scientific Rep* (2024) 14(1):8947. doi:10.1038/s41598-024-59716-x

25. Lovric G, Barré SF, Schittny JC, Roth-Kleiner M, Stampanoni M, Mokso R. Dose optimization approach to fast X-ray microtomography of the lung alveoli. *J Appl Crystallogr* (2013) 46(4):856–60. doi:10.1107/s0021889813005591